INTERNATIONAL JOURNAL FOR NUMERICAL METHODS IN FLUIDS
*Int. J. Numer. Meth. Fluids* 2002; **40**:1365–1380 (DOI: 10.1002/fld.371)

# Computation of unsteady viscous incompressible flows in generalized non-inertial co-ordinate system using Godunov-projection method and overlapping meshes

H. Pan[‡] and M. Damodaran[*,†,§]

*Division of Thermal and Fluids Engineering, School of Mechanical and Production Engineering, Nanyang Technological University, Nanyang Avenue, Singapore 639798, Singapore*

SUMMARY

Time-dependent incompressible Navier–Stokes equations are formulated in generalized non-inertial co-ordinate system and numerically solved by using a modified second-order Godunov-projection method on a system of overlapped body-fitted structured grids. The projection method uses a second-order fractional step scheme in which the momentum equation is solved to obtain the intermediate velocity field which is then projected on to the space of divergence-free vector fields. The second-order Godunov method is applied for numerically approximating the non-linear convection terms in order to provide a robust discretization for simulating flows at high Reynolds number. In order to obtain the pressure field, the pressure Poisson equation is solved. Overlapping grids are used to discretize the flow domain so that the moving-boundary problem can be solved economically. Numerical results are then presented to demonstrate the performance of this projection method for a variety of unsteady two- and three-dimensional flow problems formulated in the non-inertial co-ordinate systems. Copyright © 2002 John Wiley & Sons, Ltd.

KEY WORDS: numerical simulation; viscous flow; unsteady flow; projection method; overlapping grid; non-inertial co-ordinate system

## 1. INTRODUCTION

The primary motivation for this study stems from the need to develop suitable numerical methods for solving the unsteady incompressible Navier–Stokes (INS) equations to model the hydrodynamic environment and to estimate the hydrodynamic forces for the control and navigation of underwater robotic vehicles (URVs) which are routinely being used for underwater applications. A number of research studies done by Yuh [1], Kalske [2] and Fossen [3]

* Correspondence to: M. Damodaran, Division of Thermal & Fluids Engineering, School of Mechanical & Production Engineering, Nanyang Technological University, Nanyang Avenue, 618644 Singapore, Singapore.
† E-mail: mdamodaran@ntu.edu.sg
‡ Currently Research Engineer, Institute of High Performance Computing, Singapore.
§ Associate Professor and Singapore-MIT Alliance Faculty Fellow.

*Received March 2001*
*Revised December 2001*

have contributed towards the estimation of forces acting on underwater bodies. However, their methods were based on the potential flow theory which is a low-order fluid dynamics model. In this work, an attempt is made to solve the incompressible laminar Navier–Stokes equations to estimate the hydrodynamic forces acting on moving underwater bodies. In the case of the underwater body moving away from other underwater structures, the environment in the vicinity of the underwater body can be modelled as that of a rigid body moving in an infinite domain. In this situation a body-fixed co-ordinate system can be used with the computational domain fixed on the moving rigid body. In this case then a variable boundary condition problem is formulated instead of the moving boundary problem so that the complexities associated with the moving boundary problem can be avoided with minimum computational effort. In the case that the moving underwater body is in the vicinity of a fixed structure, then the environment can be modelled as a moving boundary problem.

There are many methods for solving the INS equations with fixed boundary conditions. However, only relatively few studies have dealt with the solution of INS equations with moving boundaries, i.e. such as that of Ogawa and Ishiguro [4] who derived the INS equations in general moving co-ordinates and solved the equations by finite difference method and Ren and Balchen [5] who solved the INS equations on the body-fixed co-ordinate system by using finite element method. In this study, the main ideas for the numerical solution of the generalized INS equations in moving-body-fixed co-ordinate system using a second-order projection method on overlapped structured grids is outlined.

It is reasonable to assume that the fluid around the body is incompressible. The main computational difficulty for simulating the incompressible flow by using the numerical method arises from the fact that the continuity equation contains only velocity components and there is no obvious link with the pressure as in the case of compressible flow, where the density carries on the link. One method, which is the focus of the current investigation for solving these equations is the second-order Godunov-projection method introduced by Bell *et al.* [6, 7] and developed by Bell *et al.* [8] and Almgren *et al.* [9]. In this projection method, a structured grid is used to discretize the flow domain in the physical space, which can be transformed to the computational space, which is a unit square in two-dimensional space or a unit cubic in three-dimensional space through a mapping $\Phi$ given by

$$\Phi = \frac{\partial(x, y, z)}{\partial(\xi, \eta, \zeta)}$$

where $(x, y, z)$ stands for the co-ordinates of the physical space and $(\xi, \eta, \zeta)$ denotes the co-ordinates of the computational space. The unsteady incompressible Navier–Stokes equations in the generalized curvilinear co-ordinate system are defined as follows:

$$\nabla_\xi \cdot \bar{\mathbf{U}} = 0 \tag{1}$$

$$\mathbf{U}_t + \frac{1}{J}(\bar{\mathbf{U}} \cdot \nabla_\xi)\mathbf{U} = \frac{\varepsilon}{J} \nabla_\xi \cdot \left[\frac{1}{J} TT^t \nabla_\xi \cdot \mathbf{U}\right] - \frac{1}{J} T^t \nabla_\xi \phi + \mathbf{F} \tag{2}$$

where $J = \det|\Phi|$, $T = J\Phi^{-1}$, $\bar{\mathbf{U}} = T\mathbf{U}$, $\varepsilon$ is the kinematic viscosity, $\mathbf{U}$ represents the velocity field and $\phi$ stands for the hydrodynamic pressure. The source term $\mathbf{F}$ appearing in the equation is the consequence of the formulation of the equations in the non-inertial co-ordinate system

 

and takes the form shown in References [10, 5] as follows:

$$\mathbf{F} = -(\dot{\mathbf{v}}_1 + \dot{\mathbf{v}}_2 \times \mathbf{r} + \mathbf{v}_2 \times \mathbf{v}_1 + \mathbf{v}_2 \times (\mathbf{v}_2 \times \mathbf{r}) + 2\mathbf{v}_2 \times \mathbf{U}) \tag{3}$$

where $\mathbf{r}$ is the position vector relative to the inertial co-ordinate system, $\mathbf{v}_1 = (u_0, v_0, w_0)^t$ and $\mathbf{v}_2 = (p, q, r)^t$ are the linear velocity and the angular velocity of the origin of the non-inertial co-ordinate frame, respectively, and $\dot{\mathbf{v}}_1$ and $\dot{\mathbf{v}}_2$ are the rates of change of the linear velocity and angular velocity of the non-inertial co-ordinate frame. By comparing Equation (2) with the conventional Navier–Stokes equation in the inertial co-ordinate system, it can be seen that the difference lies in the presence of additional source term $\mathbf{F}$, which contains the Coriolis and centripetal acceleration terms. The Godunov-projection method must therefore be modified accordingly so that the source terms can be represented in the formulation.

This projection method consists of fractional time steps. First, the momentum equation (2) is solved with a lagged pressure term to determine an intermediate velocity field, which does not satisfy the continuity equation (1). Then this intermediate velocity field is decomposed into two parts, i.e. a divergence-free and a curl-free part which define the new velocity field and an update for the pressure is done, respectively. The Godunov procedure is incorporated in the differencing of the convective terms in order to provide a robust discretization so that the restriction of cell Reynolds number can be removed.

In order to simplify the grid generation task for complex flow domain that are common for the underwater applications, a system of overlapping grids is used to discretize the computational domain. The overlapping grid consists of several component grids that overlap each other and the union of the component grids covers the whole region over which the computation is carried out. Each component grid can be generated separately and has its own mapping function. The benefits of using an overlapping system of grids are many in that it facilitates a smooth transformation for each component grid, simplifies the task of grid generation in complex geometric domains and reduces the computational overhead for solving moving boundary problems, which will be addressed in another paper. The methodology for generating the overlapping grids for the computations reported in this work follows closely the method outlined in Reference [11].

In this study the Godunov-projection method is implemented on overlapping grids to simulate moving boundary problems by solving the unsteady incompressible Navier–Stokes equations in the non-inertial co-ordinate system.

In the subsequent sections of this paper, the details of the Godunov-projection method is presented as a three-step procedure covering aspects of temporal discretization, spatial discretization and projection. This is then followed by a brief outline of the overlapping grid. Selected numerical simulations of a number of two- and three-dimensional problems are then presented and discussed.

## 2. GODUNOV-PROJECTION METHOD

The Godunov-projection method of Bell *et al.* [6] applies high order upwind schemes to provide a robust differencing scheme for the convective terms in the INS equations solved by fractional step methods as described in References [12, 13]. The Godunov procedure, which was introduced for gas dynamics by Colella [14], is incorporated in this method. The implementation of this algorithm is carried out in three steps. In the first step, the

 

second-order Godunov method is used to approximate the conservative differences of the non-linear convective terms $1/J(\bar{\mathbf{U}} \cdot \nabla_\xi)\mathbf{U}$. In the second step, the intermediate velocity field is obtained by solving the momentum equation (2) alone and by omitting the solenoidal nature of the velocity field. Finally, an approximate projection is performed to restore the divergence-free velocity field, which satisfies Equation (1) approximately, and subsequently the hydrodynamic pressure is updated. These steps are outlined briefly below.

### 2.1. Temporal discretization

Here the second-order fractional step formulation described in Reference [7] used in the present work is briefly outlined. A vector field $\mathbf{V}$ can be uniquely decomposed into a divergence-free component and a gradient of a scalar field as follows:

$$\mathbf{V} = \mathbf{V}^{\mathrm{d}} + \nabla\psi \tag{4}$$

where $\mathbf{V}^{\mathrm{d}}$ is a divergence-free vector field and $\psi$ is a scalar. A projection operator $\mathbf{P}$ can then be defined as $\mathbf{P} = \mathbf{I} - \nabla(\nabla \cdot \nabla)^{-1}\nabla$ so that $\mathbf{PV} = \mathbf{V}^{\mathrm{d}}$ and $\nabla\psi = (I - \mathbf{P})\mathbf{V}$.

By using the projection, the incompressible Navier–Stokes Equations (1) and (2) can be written as follows:

$$\mathbf{U}_t = \mathbf{P}\left(\frac{\varepsilon}{J}\nabla_\xi \cdot \left[\frac{1}{J}TT^t\nabla_\xi \cdot \mathbf{U}\right] - \frac{1}{J}(\bar{\mathbf{U}} \cdot \nabla_\xi)\mathbf{U} + \mathbf{F}\right) \tag{5}$$

By applying the Crank–Nicolson scheme for temporal discretization, Equation (5) takes the following discretized form:

$$\Delta t^{-1}(\mathbf{U}^{n+1} - \mathbf{U}^n) = \mathbf{P}\left(\frac{\varepsilon}{2J}\nabla_\xi \cdot \left[\frac{1}{J}TT^t\nabla_\xi \cdot (\mathbf{U}^{n+1} + \mathbf{U}^n)\right] - \frac{1}{J}(\bar{\mathbf{U}} \cdot \nabla_\xi)\mathbf{U}^{n+1/2} + \mathbf{F}^{n+1/2}\right) \tag{6}$$

In view of the non-local behaviour of the projection, the linear algebra problem associated with solving this equation would be very costly. As an economic alternative, a fractional step method can be applied where lagged pressure field is used for the computation. An intermediate velocity field $\mathbf{U}^*$ is computed by solving the momentum equation along with lagged pressure and then the projection is applied on the intermediate velocity field for obtaining the divergence-free velocity field $\mathbf{U}^{n+1}$ and update of the pressure field. A number of forms for projection exist and according to the analysis carried out by Rider [15] and Almgren *et al.* [16], the pressure form of projection is the most robust as there is no accumulation of the error associated with the no divergence assumption. In view of this the intermediate velocity field is computed by solving the following equation and subsequently corrected by the gradient of pressure:

$$\Delta t^{-1}(\hat{\mathbf{U}}^{*,n+1} - \mathbf{U}^n) = \frac{1}{2}J^{-1}\varepsilon\nabla_\xi \cdot [J^{-1}TT^t\nabla_\xi \cdot (\hat{\mathbf{U}}^{*,n+1} + \mathbf{U}^n)] - J^{-1}[(\bar{\mathbf{U}} \cdot \nabla_\xi)\mathbf{U}]^{n+1/2} - J^{-1}T^t\left(\frac{\nabla_\xi\phi}{\rho}\right)^{n-1/2} + \mathbf{F}^{n+1/2} \tag{7}$$

 

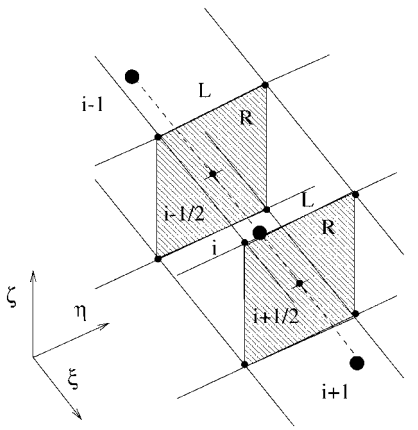


Figure 1. Location of cell- and face-centred variables.

then

$$\mathbf{U}^{*,n+1} = \hat{\mathbf{U}}^{*,n+1} + \Delta t J^{-1} T^t (\nabla_\xi \phi)^{n-1/2} \tag{8}$$

Next a projection is applied for decomposing the vector field into a divergence-free component and a curl-free component so as to obtain a new velocity field $\mathbf{U}^{n+1}$ and to update the pressure gradient $J^{-1}T^t(\nabla_\xi \phi/\rho)^{n+1/2}$.

### 2.2. *Spatial discretization*

The spatial discretization of the momentum equation (2) is based on a cell-centred approximation since this arrangement provides the most natural setting for implementing the Godunov method. The diffusion term can be discretized by using the standard second-order central difference in the computational space and the non-linear convective term is discretized by the second-order Godunov method in order to provide a robust approximation.

Figure 1 shows a schematic of a three-dimensional grid with the co-ordinate indices defining cell centres and cell faces. In order to compute the flux on the faces of cell, the velocity on the faces is extrapolated from the values computed at the cell centres. Since this method is also second-order accurate in time direction, the flow variables are extrapolated both in space and time using Taylor series expansion. After combining the derivative in the normal direction, the following equations are used to extrapolate the velocity $\mathbf{U}$ on the faces $(i+1/2, j, k)$

$$\mathbf{U}_{i+1/2}^{n+1/2,L} = \mathbf{U} + \left[\frac{\Delta\xi}{2} - \frac{\Delta t}{2J}\,\bar{u}\right]\mathbf{U}_\xi - \frac{\Delta t}{2J}(\bar{v}\mathbf{U}_\eta + \bar{w}\mathbf{U}_\zeta)$$
$$+ \varepsilon\left[\frac{\Delta t}{2J}\,\nabla_\xi\left(\frac{1}{J}\,TT^t\nabla_\xi \cdot \mathbf{U}\right)\right] - \frac{\Delta t}{2J}\,T^t\nabla_\xi\phi + \mathbf{F} \tag{9}$$

 

$$\mathbf{U}_{i+1/2}^{n+1/2,R} = \mathbf{U}_{i+1} - \left[\frac{\Delta\xi}{2} + \frac{\Delta t}{2J}\bar{u}_{i+1}\right](\mathbf{U}_\xi)_{i+1} - \frac{\Delta t}{2J}(\bar{v}\mathbf{U}_\eta + \bar{w}\mathbf{U}_\zeta)_{i+1} + \varepsilon\left[\frac{\Delta t}{2J}\nabla_\xi\left(\frac{1}{J}TT^t\nabla_\xi\cdot\mathbf{U}_{i+1}\right)\right] - \frac{\Delta t}{2J}T^t(\nabla_\xi\phi)_{i+1} + \mathbf{F}_{i+1} \tag{10}$$

where $\mathbf{U} = \mathbf{U}_{i,j,k}^n$ and $\mathbf{U}_{i+1/2}^{n+1/2} = \mathbf{U}_{i+1/2,j,k}^{n+1/2}$, etc. are implied by the subscript indices. A slope limiter, such as superbee and minmod limiter, can be used to estimate the gradient of the flow variables in the cell in each co-ordinate direction. The variable has two values, one of which is extrapolated from left cell and the other from the right cell. The extrapolation is handled by using a Riemann solver, where an upwind averaging is applied. It is also possible to employ an approximate Riemann solver presented in Reference [17]. It should be noted that the pressure terms appearing in Equations (9) and (10) are not used in this extrapolation in view of the weak instability which had been observed by Lai [18] if lagged pressure terms and if the CFL number is greater than 0.5. Hence the marker-and-cell (MAC) projection method outlined in Reference [19] is used so that the resulting velocity field on the staggered grid is divergence-free. The convective terms are discretized as follows:

$$\left(\frac{1}{J}[(\bar{\mathbf{U}}\cdot\nabla_\xi)\mathbf{U}]\right)^{n+1/2} \approx \frac{(\bar{u}_{i+1/2} + \bar{u}_{i-1/2})}{2J}\frac{(\mathbf{U}_{i+1/2} - \mathbf{U}_{i-1/2})}{\Delta\xi} + \frac{(\bar{v}_{j+1/2} + \bar{v}_{j-1/2})}{2J}\frac{(\mathbf{U}_{j+1/2} - \mathbf{U}_{j-1/2})}{\Delta\eta} + \frac{(\bar{w}_{k+1/2} + \bar{w}_{k-1/2})}{2J}\frac{(\mathbf{U}_{k+1/2} - \mathbf{U}_{k-1/2})}{\Delta\zeta} \tag{11}$$

where the superscript $n + \frac{1}{2}$ is omitted from the terms in the RHS of the equation for convenience.

### 2.3. *Projection*

The final step of this projection algorithm decomposes the vector field into a divergence-free component and a gradient of scalar quantity. The projection is defined by the divergence operator $D$ and gradient operator $G$ as in References [20, 7], which satisfy the property:

$$(D\mathbf{V}, \psi)_\mathrm{s} = -(\mathbf{V}, G\psi)_\mathrm{v} \tag{12}$$

where the terms $(\cdot,\cdot)_\mathrm{s}$ and $(\cdot,\cdot)_\mathrm{v}$ represent the appropriate inner products on the discrete spaces of scalars and vectors, respectively. This condition guarantees that the numerical projection is orthogonal. Exact discrete projection utilizes the central difference for both $D$ and $G$ operators and the discrete Laplacian operator derived decouples the grid [21] as shown in Figure 2, where a two-dimensional grid is decoupled into four distinct subgrids. Almgren *et al.* [9] introduced an approximate projection, which kept the same discrete form of the Poisson equation so that it can take advantage of the fast solvers. However, the resulting divergence-free component is not really divergence-free even though its divergence is of the order $O(h^2)$ as reported in Almgren *et al.* [9].

 

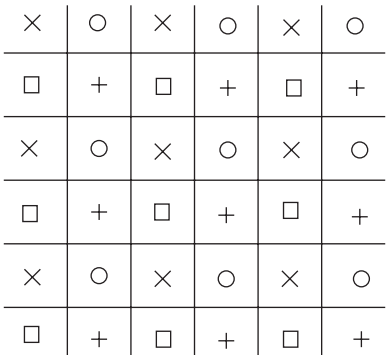

Figure 2. This figure shows the four decoupled grids for a two-dimensional grid.

Since the pressure form of projection is adopted in this section, $\mathbf{U}^{*,n+1}$ is projected to extract the following linear system:

$$L_{\mathrm{st}}\psi = D\left(\frac{\mathbf{U}^{*,n+1}}{\Delta t}\right) \tag{13}$$

where $L_{\mathrm{st}}$ represents the standard difference Laplacian operator and the equations used to compute the new velocity field and the gradient of pressure are as follows:

$$\frac{\mathbf{U}^{n+1}}{\Delta t} = \frac{\mathbf{U}^{*,n+1}}{\Delta t} - G\psi$$

$$\frac{1}{J}\,T^t \nabla_\xi \phi^{n+1/2} = G\psi$$

### *2.4. Estimation of pressure field*

It is important to estimate the pressure field from the velocity field so that forces induced by fluid flow can be estimated. It is noted that as the pressure at half-time step is computed in the numerical scheme outlined in the previous sections, the pressure at each time level is not available. Hence a separate procedure is incorporated into the algorithm to obtain the pressure field after computing the velocity field. The pressure Poisson equation which is obtained by taking the divergence on both sides of the momentum equation (2) and also by considering the satisfaction of the divergence-free property of the velocity field as follows:

$$\frac{\nabla \cdot (\nabla \phi)}{\rho} = -\nabla \cdot (\mathbf{U} \cdot \nabla)\mathbf{U} + \nabla \cdot \mathbf{F} \tag{14}$$

## 3. OVERLAPPING GRID

A system of overlapping grids is used to simplify the grid generation task for geometrically complicated flow domains. Even though the geometry of the test cases considered in this work are relatively simple the aim of this work is to demonstrate the implementation of the

 

algorithm on overlapping grids and to gain confidence before applying this method to more complex geometries. The overlapping grid consists of several component grids, which overlap each other. Since it is not required to match on the interior boundaries between the component grids, the grid generation can be more flexible so that the cost for constructing the structured grid for complex flow simulation problems can be greatly reduced. However, the overlap region between the component grids must be large enough so that the flow information can be transferred between component grids correctly. Chesshire and Henshaw [11] described a method for generating such overlapping grids and a procedure for determining interpolation coefficients to enable flow variable transfer and interpolation. The grid generator, Ogen outlined in Reference [22], is used to generate the overlapping grids used in this work. The internal boundary of component grid consists of the interpolation cells whose flow variable values are extracted from other component grids with which it overlaps with.

For overlapping grid, each component grid has its own mapping function $\Phi$. Hence Equations (1) and (2) can be set up on each component grid and the Godunov-projection algorithm outlined here can be applied on each component grid provided the values on the interior boundary are known. Hence, the flow fields on the component grids are coupled to the flow variables on the interior boundary cells. In this work, a high order interpolation is used to compute the flow variables on the interior boundary cells. In this study a third-order interpolation for the implementation of the approximate projection method is used so as to maintain the divergence of the projected velocity field to second order $O(h^2)$. This is shown in Reference [11] which shows that a third-order interpolation is required in order to retain the overall second-order accuracy of the Godunov-projection method for the solution of the incompressible Navier–Stokes equations.

The Godunov-projection method is applied on the overlapping grid by employing the original difference method on every component grid and using the interpolation equation on the interior boundary cells. The resulting system of linear equations from all the cells of the overlapping grid are solved simultaneously using various iterative methods such as the quasi-minimum residual (QMR) method in the construction of the evolving numerical flow field. The use of overlapping grids can also reduce the computational cost for computing flows with moving boundaries. In the evolution of the flow field, the modified computational grid can be regenerated cheaply by moving the component grids around the rigid body according to the motion of the body and recomputing the interpolation relations between the background grids and the body grids.

## 4. NUMERICAL RESULTS

The Godunov-projection algorithm as outlined in the previous sections has been implemented on overlapping grids for some standard benchmark flow problems in the inertial co-ordinate system as showcased in Reference [23]. In order to demonstrate the performance of the Godunov-projection method on the body-fixed co-ordinate system, two benchmark problems are solved. A moving boundary problem, where a cylinder moves in a tank, is simulated to show the procedure of using overlapping grids to solve moving boundary problem. This is followed by the computation of flow around an oscillating cylinder where the body-fixed co-ordinate system has been used for the formulation of the problem. The algorithm is also applied to compute the flow around a multi-bodied under-water robotic vehicle prototype

 

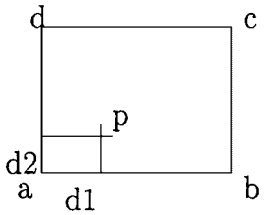


Figure 3. Interpolation scheme.

undergoing an accelerated motion schedule and based on this computation, added mass coefficients that are normally estimated from experimental data for supplementing low-order hydrodynamic models are estimated approximately.

### *4.1. Flow around moving body in a tank*

One of the prime challenges in simulating a moving boundary problem in fluid flow concerns with the manner in which the computation is carried out in computational domain which changes shape with time. One particular model flow problem resembling the motion of bodies underwater that has been solved by Ren [5] using a Finite Element Method for solving the INS is repeated here with the present algorithm to demonstrate the capability of using overlapping grid to simulate the moving boundary problem. The Godunov-projection algorithm for solving the INS Equations in a body-fixed co-ordinate system is used to examine the implications for more realistic three-dimensional hydrodynamic flow problems. Two co-ordinate-systems, namely the tank-fixed co-ordinate system and the body-fixed co-ordinate system exist for consideration in the simulation of this problem. Since the most interesting area of computational domain is the area around the moving body and the tank has a simple rectangular geometry, one possible method for simulating the problem is to solve the INS equations in the body-fixed co-ordinate system so that there is no need for interpolating the flow field variables on the body grid and hence a more accurate solution can be expected from the simulation. In order to facilitate this approach two sets of grids are generated and overlapped, i.e. a body grid is generated around the cylindrical body and is overlapped on the rectangular tank grid. The motion of body is then represented by moving the tank grid instead of the grid around the cylinder. When the tank grid is moved, an overlapping grid is regenerated by establishing the interpolation relationship between the new tank grid and the body grid. The flow variables on the body grid can be kept and only the variables on the new tank grid are obtained to be interpolated from that on the previous overlapping grid. This results in a reduction of the computational overhead. At a given instant of time, the computational procedure for solving the moving boundary problem begins with the solution being advanced using a time step without moving any grid. Next, the tank grid is moved by the distance traversed during the time step in the body-fixed co-ordinate system. This is followed by regenerating the interpolation relationship between the new tank grid and the body grid. Then, the flow variables on the new tank grid are redistributed by interpolating from the previous overlapping grid. The computation is advanced to the next time-step. The interpolation scheme to redistribute the flow field in the tank grid is briefly outlined here. As shown in Figure 3, the interpolation is done in the computational space $(\xi, \eta)$, where $\Delta\xi$

 

and $\Delta\eta$ are both unity and points $a, b, c$ and $d$ are the nodal points forming a cell in which the point $p$ at which values are to be interpolated lies in. Bilinear interpolation is used to estimate the interpolated value as follows:

$$u_p = (1 - d_2)[(1 - d_1)u_a + d_1 u_b] + d_2[(1 - d_1)u_d + d_1 u_c]$$

For this simulation, the moving body is a circular cylinder with a diameter $d = 0.2$ m and the tank is a rectangle $2 \times 1.2$ m. The body moves with $u_0 = 0.1$ m/s and $v_0 = 0$ in the tank-fixed co-ordinate system. The Reynolds number is set to 175. As the computation is done on the body-fixed co-ordinate system the tank moves with $u_{\Gamma_{\text{tank}}} = -0.1$ m/s. The initial computational domain and the component grids are shown in the Plate 1(a), which contains two component grids, one being the uniform grid having $85 \times 45$ cells discretizing the fluid domain in the rectangular tank and the other being the O-grid around the cylinder having $49 \times 17$ cells and with grid lines clustered in the vicinity of the cylinder surface. Initially, the velocity field is assumed to be uniform field with value of $u_{\Gamma_{\text{tank}}}$. This corresponds to a stationary initial flow field in the tank-fixed co-ordinate system. Plate 1(b) shows the orientation of the overlapping grid after time $t = 5$ has elapsed from the initial state. It can be seen that the tank grid has changed its position. The computed flow field of the cylinder moving in a tank at the same instant, $t = 5$, is shown in Plate 2. The computed streamline pattern on the body-fixed co-ordinate system is shown in Plates 2(a) and 2(b) shows the computed pressure contours at this instant. From these figures the formation of vortices in the wake of the cylinder can be seen although the vortex shedding process has not yet been initiated yet. The vorticity contour plot shown in Plate 2(c) confirms this observation. As the computed results agree well with those reported in Reference [5], the feasibility of this approach involving the implementation of the Godunov-projection algorithm on overlapped grids for the solution of the INS in non-inertial co-ordinate systems has been demonstrated.

### *4.2. Flow around a oscillating circular cylinder*

The computation of unsteady flow past a bluff body has received enormous attention especially for the prediction of the loads on engineering structures, such as pipelines and offshore platform. The wake vortices also interact with the structure and induce oscillating lift and drag forces whose frequencies are directly related to the vortex shedding frequency. The transverse oscillation of cylinder with a frequency at or near its natural vortex shedding frequency, which is defined as the frequency of vortex shedding when the flow past a stationary cylinder, causes vortex shedding to occur at the frequency of cylinder oscillation and result in an increase in the mean value of the drag. This phenomenon of fluid-structure interaction is known as 'lock-in' or 'wake capture'. Similarly, the in-line oscillation of the cylinder with a frequency at or near twice the natural vortex shedding frequency increases the lift amplitude and induces the vortex shedding to occur at half the frequency of cylinder oscillation. There are several experimental and numerical investigations of transverse or in-line oscillating cylinders, such as References [24–26] and the lock-in zones of frequency at various Reynolds numbers and amplitude of oscillation have been studied also.

Here the flow past an oscillating circular cylinder is considered as a benchmark problem to verify the results predicted by modified Godunov-projection method on overlapping grids. The circular cylinder is immersed in a uniform flow and oscillates either in the transverse ($y$-axis) or lateral (in-line or $x$-axis) direction at a frequency close to its natural frequency.

 

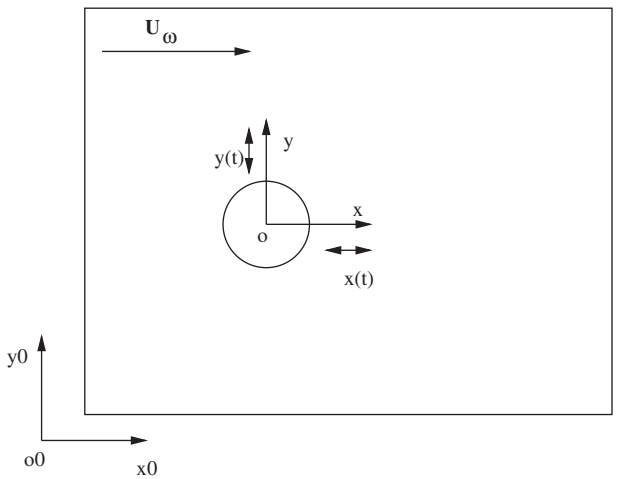


Figure 4. Configuration of the flow past an oscillating cylinder.

The Reynolds number for the flow is based on the uniform free-stream velocity. The cylinder is assumed to be stationary initially and is forced to oscillate sinusoidally after the alternating vortex shedding process has been initiated and established. The configuration of the computational domain and the co-ordinate systems are shown in Figure 4. The inflow boundary is located 8 diameters ahead the cylinder and the outflow boundary at 24 diameters aft of the cylinder. The top and bottom far-field boundaries are 8 diameters away from the cylinder. At the far-field boundaries the velocity is specified as the undisturbed free stream velocity. The oscillation of cylinder is defined by the following equations:

$$\text{In-line oscillation: } x(t) = -a_x \cos[2\pi f_x(t - t_p)]$$

$$\text{Transverse oscillation: } y(t) = -a_y \cos[2\pi f_y(t - t_p)]$$

where $a_x$ and $a_y$ are the amplitude of oscillation, $f_x$ and $f_y$ are the frequencies of oscillation and $t_p$ is the time when the cylinder starts to oscillate. A system of overlapping grids for this calculation consists of a circular grid and a background rectangular grid. The circular grid, whose outer diameter is 6 times of cylinder diameter, consists of $56 \times 32$ cells and the background grid consists of $120 \times 88$ grid cells. The grid cells are clustered around the cylinder. As the non-inertial reference frame attached the cylinder, $xoy$, is used, the grid is fixed during the calculation.

In order to verify the computed results, the test cases computed and reported in Reference [25] who uses a different approach are simulated. The current algorithm is used to compute the unsteady flow around a cylinder which oscillates both in the transverse and lateral directions. The Reynolds number of the flow is based at 100 and the Strouhal number corresponding to the natural vortex shedding frequency is $St_n = f_n D/U_\infty = 0.164$. The cylinder oscillates simultaneously in the in-line and transverse directions with frequency parameters $f_x = 2f_y = 2f_n$ and the amplitude of the oscillation in the in-line and transverse direction is $a_x = a_y = 0.2D$ and corresponds to those values used in the studies carried out by Karanth [25]. The contour plots of computed pressure and vorticity corresponding to a well-developed flow field at an

 

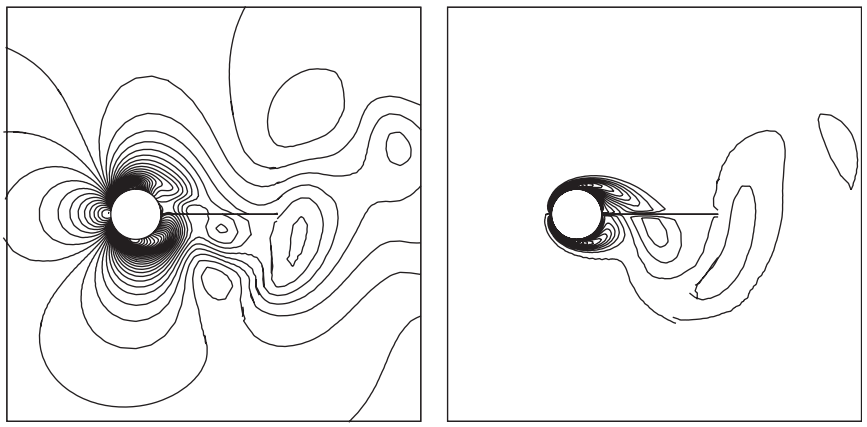

(a) pressure (a) vorticity

Figure 5. Pressure and vorticity contour plots of flow past a cylinder with combined oscillation, $f_x = 2f_y = 2f_n$, $a_x = a_y = 0.2D$.

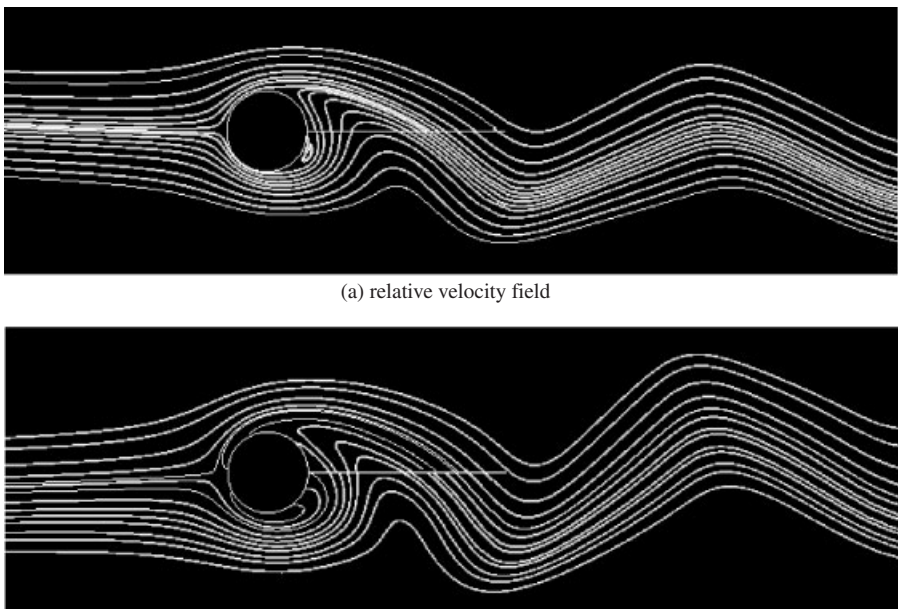

(a) relative velocity field

(b) absolute velocity field

Figure 6. Streamlines of relative and absolute velocity field of flow past a cylinder with the combined oscillation, $f_x = 2f_y = 2f_n$, $a_x = a_y = 0.2D$.

instant of time are shown, respectively, in Figures 5(a) and 5(b). It can be seen that the vortex shedding arises in the wake of cylinder. The streamlines of relative and absolute velocity field at the same instant of time are shown in Figure 6. The time-variation of the computed lift and drag coefficients are shown in Figure 7. The variation of lift with time does not correspond to

 

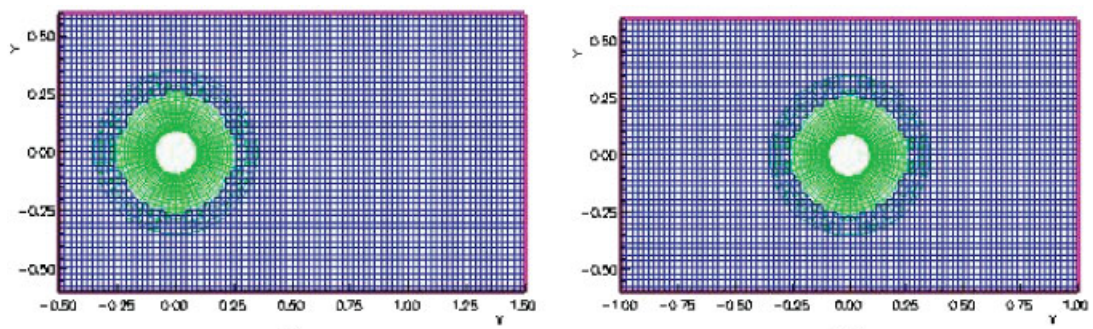


Plate 1. Overlapping grids for flow around moving body in a tank: (a) $t = 0$; (b) $t = 5$.

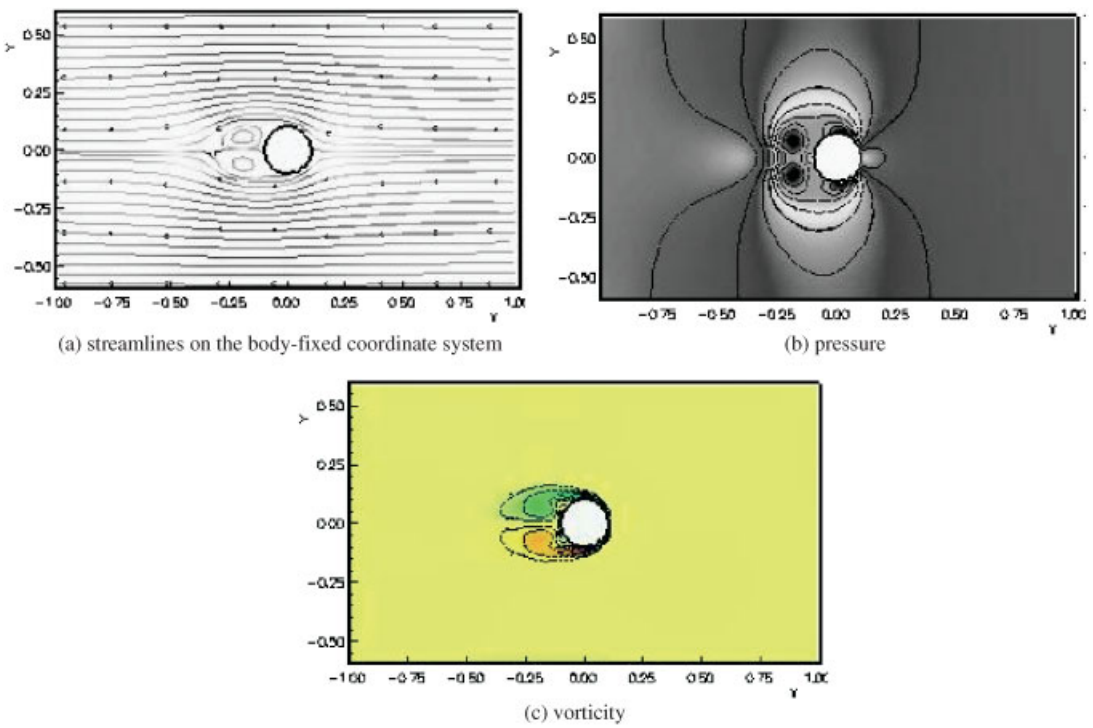


Plate 2. Flow field of the cylinder moving in a tank at $t = 5$.

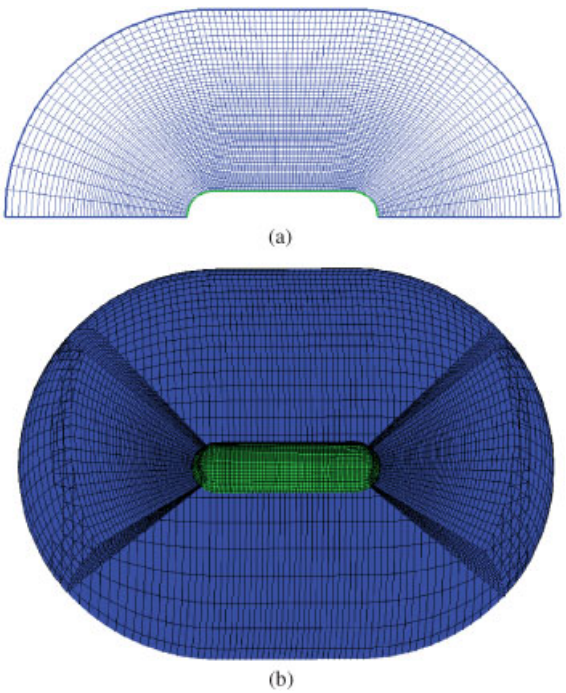


Plate 3. Section grids for the mainbody: (a) section grid for the mainbody; (b) near-field grids around the mainbody.

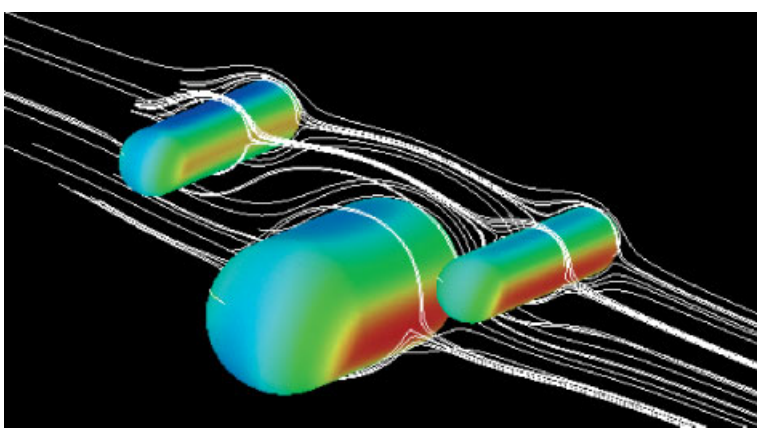

Plate 4. Instantaneous pressure and streamline plots of the flow corresponding to URV accelerating along the lateral axis.

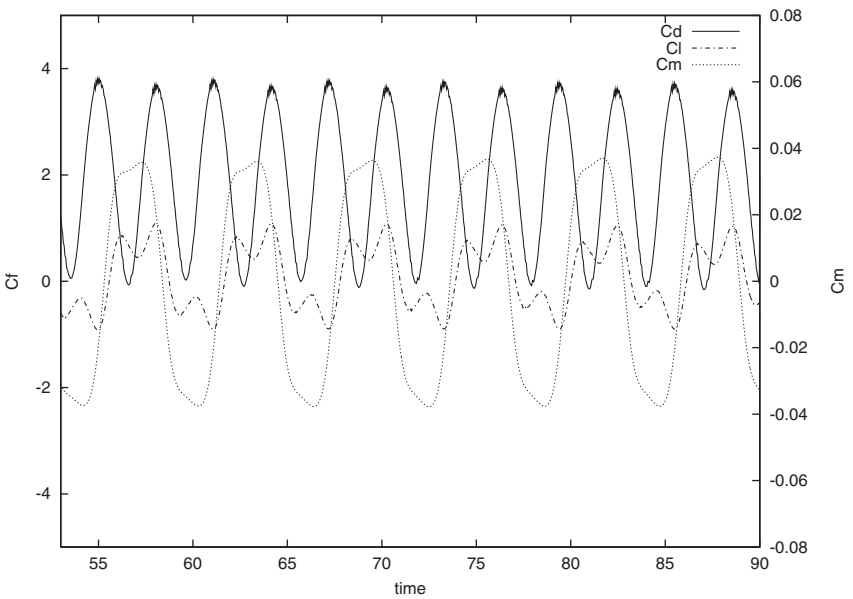


Figure 7. Time variation of force coefficients of cylinder with combined oscillation, $f_x = 2f_y = 2f_n$, $a_x = a_y = 0.2D$.

a sinusoidal variation. From the graph the estimate of the mean drag coefficient $C_{d,m}$ is 1.77 and the amplitude of the drag coefficient is $C_{d,\mathrm{amp}}$ is 1.89. The estimate of the maximum lift coefficient $C_{l,\max}$ is 0.978. These quantities are in close agreement with the results reported in Reference [25].

### *4.3. Unsteady flow around an accelerating URV*

The algorithm is next extended for the unsteady flow past a multi-bodied URV prototype which contains three bodies, namely a main body and two buoyant tubes. An overlapping grid is generated to discretize the complex computational domain around the multi-bodied URV, which includes component grids around the three bodies and a background grid. A hierarchical structure is used so that the component grids of the two buoyant tubes are totally embedded in the component grids of main body and the background grid only overlaps with the main body grids, which, in turn, is associated with the tube grids. Hence, the computational costs for estimating the interpolation relationship can be greatly reduced. Figure 8 shows this hierarchical structure. For each body by virtue of its symmetry, a cylindrical grid is constructed by rotating a two-dimensional section grid and two head grids are used to remove the singular grid points which lie on the axis around which the sectional grids have been rotated. Plate 3 shows the sectional grid and the near-field grid system around the main body, which also show these head grids. Similar grids are also constructed in the domains around the two buoyant tubes. The background grid is a Cartesian grid, which covers overall extent of the computational area around the multi-bodied geometric configuration. The total number of grid cells used for this three-dimensional flow problem is about 1.2 million cells. Since the number

 

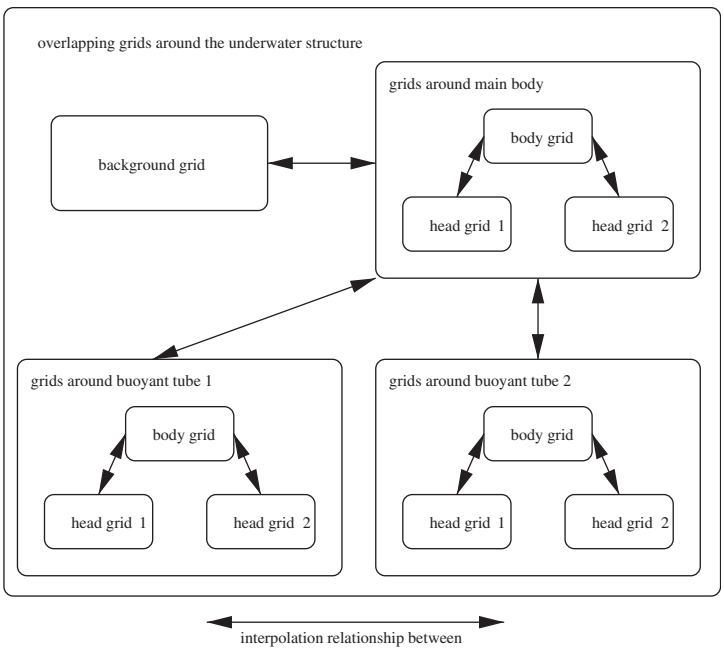


Figure 8. Hierarchical structure of overlapping grid for underwater vehicle.

of grid cells is very large, for computing this flow economically, the flow algorithm has been parallelised to run on a multi-processor computer as outlined in a related paper by Pan and Damodaran [23].

The estimation of hydrodynamic forces and moments acting on the URV is essential for the construction of the control system for its navigation and control in underwater operations. In other words, all hydrodynamic coefficients have to be determined. The CFD simulation based on the current algorithm can be used to estimate these coefficients in situations where there is no direct access to experimental hydrodynamic simulation facilities. The Godunov-projection algorithm has been used to solve the flow past the underwater vehicle and to estimate the hydrodynamic coefficients. Low-order hydrodynamic models based on potential flow theory are usually supplemented with the so-called 'added mass' coefficients estimated from experimental data from water-tunnels for extending the range of their validity and realism. In situations where it is not possible to have access to experimental data, it is possible to extract these 'added mass' coefficients from numerical solutions of the INS equations. It can be assumed that both vehicle and fluid are still or in some steady-state motion initially and the URV is set in sudden motion according to some prescribed motion which may be steady motion in another direction or an unsteady (accelerated) motion or a combination of translational and rotational motion prescribed, respectively, as a function of time along or about the lateral, star-board and/or vertical direction. Since the velocity of the vehicle is low and if it is reasonable to assume that the forces are caused mainly by the acceleration of vehicle, then the approximation of the 'added mass' coefficients can be computed from the unsteady flow fields simulated by the Godunov-projection algorithm.

 

Table I. Added mass coefficients of the multi-body underwater vehicle.

| | | |
|---|---|---|
| *Hydrodynamic coefficients on* $\dot{u}$ | | |
| $X_{\dot{u}} = 2.15 \times 10^{-2}$ | $Y_{\dot{u}} = 0$ | $Z_{\dot{u}} = 0$ |
| $K_{\dot{u}} = 0$ | $M_{\dot{u}} = 1.32 \times 10^{-3}$ | $N_{\dot{u}} = 0$ |
| *Hydrodynamic coefficients on* $\dot{v}$ | | |
| $X_{\dot{v}} = 0$ | $Y_{\dot{v}} = 5.82 \times 10^{-2}$ | $Z_{\dot{v}} = 1.07 \times 10^{-4}$ |
| $K_{\dot{v}} = -4.70 \times 10^{-3}$ | $M_{\dot{v}} = 0$ | $N_{\dot{v}} = -2.04 \times 10^{-2}$ |
| *Hydrodynamic coefficients on* $\dot{w}$ | | |
| $X_{\dot{w}} = 0$ | $Y_{\dot{w}} = 0$ | $Z_{\dot{w}} = 6.84 \times 10^{-2}$ |
| $K_{\dot{w}} = 0$ | $M_{\dot{w}} = 2.26 \times 10^{-2}$ | $N_{\dot{w}} = 0$ |

Plate 4 shows the computed flow field at an instant of time when the URV is made to accelerate along the direction parallel to the lateral axis. The computed pressure contours and streamline pattern at selected sectional planes are shown in this figure. The colors on the body surfaces and streamlines are calibrated according to the local value of the pressure. High pressure appears on the upwind side of the vehicle and low pressure on the downwind side. As the velocity of the vehicle is still low, no vortices have been formed at this instant of time. From the computed flow fields such as these at a particular instant of time, added mass coefficients can be estimated for cases when the URV is in accelerated motion along its longitudinal, lateral and vertical axis. Table I shows the values of these added mass coefficients estimated from the computational flow field. In this table the notations $X_{\dot{u}}$ and $Y_{\dot{u}}$, etc. are defined according to the definitions in Reference [2] and refer to the added mass coefficients along the three body co-ordinate directions. In the same manner, other hydrodynamic coefficients can also be obtained by performing the flow simulation at the specific instants of time.

## 5. CONCLUSION

In this work, a modified Godunov-projection method implemented on a system of overlapping grids for solving the unsteady incompressible Navier–Stokes equations in the non-inertial co-ordinate system has been described. This scheme is second-order accurate both in time and space. The Godunov procedure is incorporated to provide a robust discretization of the convection term for high Reynolds number flow. The pressure Poisson equation is solved to obtain the pressure field. The extra source term arising from the formulation in non-inertial co-ordinate system can be easily incorporated into the numerical scheme. The use of overlapping grids not only makes grid generation easier, but also reduces the computational cost for solving the moving boundary problems encountered in the underwater hydrodynamic applications. It can be concluded based on the benchmark time-dependent flow problems that the Godunov-projection algorithm when combined with a system of overlapping grids and implemented on parallel computers, can serve as a feasible prediction tool for hydrodynamic modelling for simulating the navigation and control of underwater vehicles. In the future the algorithm can be coupled with a six-degree-of freedom dynamics model to couple the fluid dynamics and

 

kinematics together to explore coupled field problems in which the evolving trajectories of the URVs can be predicted for a freely moving or a controlled URV interacting freely with hydrodynamic environment.

## REFERENCES


1. Yuh J. Modeling and control of underwater robotic vehicles. *IEEE Transactions on Systems, Man and Cybernetics* 1990; **20**:1475–1483.
2. Kalske S. Motion simulation of underwater vehicles. VTT-PUBS-97, Ship Laboratory, Technical Research Centre of Finland, ESPOO, Finland, 1992.
3. Fossen TI. *Guidance and Control of Ocean Vehicles*. Wiley: Chichester, NY, 1994.
4. Ogawa S, Ishiguro T. A method for computing flow fields around moving bodies. *Journal of Computational Physics* 1987; **69**:49–68.
5. Ren G, Balchen J. Finite element modeling of the hydrodynamic environment of a small ROV. *Modeling, Identification and Control* 1993; **14**(3):145–159.
6. Bell JB, Colella P, Glaz HM. A second-order projection method for viscous incompressible flow. In *AIAA Paper 87-1776-CP, Proceedings of AIAA 8th Computational Fluid Dynamics Conference*, Honolulu, Hawaii, 1987; 789–794.
7. Bell JB, Colella P, Glaz HM. A second-order projection method for the incompressible Navier–Stokes equations. *Journal of Computational Physics* 1989; **85**(2):258–283.
8. Bell JB, Solomon JM, Szymczak WG. A projection method for viscous incompressible flow on quadrilateral grids. *AIAA Journal* 1994; **32**(10):1961–1969.
9. Almgren AS, Bell JB, Szymczak WG. A numerical method for the incompressible Navier–Stokes equations based on an approximate projection. *SIAM Journal of Scientific Computing* 1996; **17**(2):358–369.
10. Pedlosky J. *Geophysical Fluid Dynamics*. Springer: New York, 1987.
11. Chesshire G, Henshaw WD. Composite overlapping meshes for the solution of partial differential equations. *Journal of Computational Physics* 1990; **90**:1–64.
12. Perot JB. An analysis of the fractional step method. *Journal of Computational Physics* 1993; **108**:51–58.
13. Peyret R, Taylor TD. *Computational Methods for Fluid Flow*. Springer: New York, 1983.
14. Colella P. A direct Eulerian MUSCL scheme for gas dynamics. *SIAM Journal on Scientific and Statistical Computing* 1985; **6**:104–117.
15. Rider WJ. Approximate projection methods for incompressible flows: implementation, variants and robustness. Los Alamos National Laboratory Technical Report LA-UR-94-2000, http://www-xdiv.lanl.gov/XHM/personnel/wjr/Webpapers/pubs.html, USA, 1994.
16. Almgren AS, Bell JB, Crutchfield WY. Approximate projection methods: Part 1: inviscid analysis. *SIAM Journal of Scientific Computing* 2000; **22**(4):1139–1159.
17. Roe PL. Approximate Riemann solvers, parameter vectors and difference schemes. *Journal of Computational Physics* 1981; **43**:357–372.
18. Lai MF, Bell JB, Colella P. A projection method for combustion in the zero mach number limit. In *Proceedings of AIAA 11th Computational Fluid Dynamics Conference*, Orlando, FL, 1993; 776.
19. Harlow FH, Welch JE. Numerical calculation of time-dependent viscous incompressible flow of fluid with free surface. *Physics of Fluids* 1965; **8**(12):2182–2189.
20. Chorin AJ. Numerical solution of the Navier–Stokes equations. *Mathematics of Computation* 1968; **22**: 745–762.
21. Minion ML. A projection method for locally refined grids. *Journal of Computational Physics* 1996; **127**: 158–177.
22. Henshaw WD. Ogen: an overlapping grid generator for overture. Technical Report LA-UR-96-3466, Lawrence Livermore National Laboratory, US, 1996.
23. Pan H, Damodaran M. Parallel computation of viscous incompressible flows using Godunov-projection method on overlapping meshes. *International Journal of Numerical Methods in Fluids* 2002; **39**:441–463.
24. Moe G, Wu ZJ. The lift force on a vibrating cylinder in a current. In *Proceedings of the 8th International Conference on Offshore Mechanics and Arctic Engineering*, 1989; 159–268.
25. Karanth D, Rankin GW, Sridhar K. Computational study of flow past a cylinder with combined in-line and transverse oscillation. *Computational Mechanics* 1995; **16**:1–10.
26. Lecointe Y. Flow structure in the wake of an oscillating cylinder. *Journal of Fluid Engineering* 1995; **111**: 139–148.


 